Dunning, G. T., Preston, T. J., Orr-Ewing, A. J., Greaves, S. J., Greetham, G. M., Clark, I. P., & Towrie, M. (2014). Dynamics of photodissociation of XeF2 in organic solvents. *Physical Chemistry Chemical Physics*, *16*(30), 16095-16102. https://doi.org/10.1039/c4cp01854k

# DYNAMICS OF PHOTODISSOCIATION OF $XeF_2$ IN ORGANIC SOLVENTS

Greg T. Dunning, Thomas J. Preston, and Andrew J. Orr-Ewing*

*School of Chemistry, University of Bristol, Cantock's Close, Bristol BS8 1TS, U.K.*

Stuart J. Greaves

*School of Engineering and Physical Sciences, Heriot-Watt University, Edinburgh EH14 4AS,U.K.*

Gregory M. Greetham, Ian P. Clark, and Michael Towrie

*Central Laser Facility, Research Complex at Harwell, Science and Technology Facility Council, Rutherford Appleton Laboratory, Harwell Science and Innovation Campus, Didcot, Oxfordshire, OX11 0QX, U.K.*

* Author for correspondence

Phone: +44 117 9287672

e-mail: a.orr-ewing@bristol.ac.uk

TABLE OF CONTENTS

This article explores photodissociation of $XeF_2$ in solution, using femtosecond pump probe spectroscopy to follow the fates of photoproducts following cleavage of one Xe-F bond.

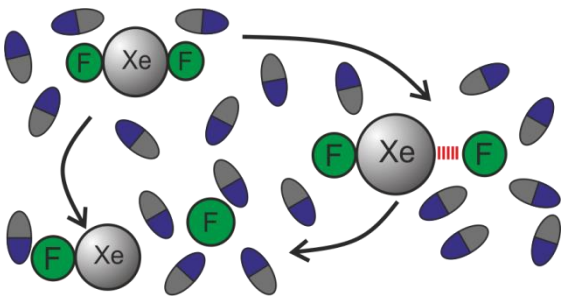

ABSTRACT

Transient electronic absorption measurements with 1-ps time resolution follow $XeF_2$ photoproducts in acetonitrile and chlorinated solvents. Ultraviolet light near 266 nm promptly breaks one Xe-F bond and probe light covering 320-700 nm monitors the products. Some of the cleaved F atoms remain in close proximity to an XeF fragment and perturb the electronic states of XeF. The time evolution of a perturbed spectral feature is used to monitor the FXe-F complex population, which decays in less than 5 ps. Decay can occur through geminate recombination, diffusive separation or reaction of the complex with the solvent.

## I. INTRODUCTION

Studying the photochemistry of small, solvated molecules presents a route to exploring the fundamental role of the surrounding medium in condensed-phase chemistry.[1] In certain cases, the photoproducts are reactive, but isolating them in an inert solvent can provide a first step to interpreting their chemistry in reactive environments. Gas-phase photolysis of the precursor we use in the present work, xenon difluoride, produces XeF and a highly reactive F atom.[2,3] Xenon difluoride itself is a strong oxidiser and effective fluorinating agent in organic and inorganic syntheses.[4,5] For example, photolysis of $XeF_2$ acts as a light-driven oxidant of gold nanoparticles.[6]

Condensed-phase photolysis can parallel its gas-phase analogue,[7,8] but the presence of the solvent can modify photodissociation dynamics in several ways. The surrounding molecules restrict the system from reaching complete separation, which can lead the nascent species to sample metastable complexes that can be non-intuitive to chemists. The solvent molecules can also affect the photochemistry by altering the electronic states involved in photolysis or by exchanging energy with the reactive complex during its separation. With small molecules

like $XeF_2$ that have known spectroscopic features[9,10] and relatively few reaction pathways,[4,5,11] we can build on our chemical intuition of condensed-phase chemistry.

Our current effort uses time-resolved transient absorption spectroscopy to determine the condensed-phase dynamics and products of $XeF_2$ from 1 ps to 1.5 ns after photodissociation. This work provides ready analysis of $XeF_2$ as a source of F atoms for use in our on-going studies of liquid-phase bimolecular reaction dynamics.[12] Following absorption of a 266 nm photon by $XeF_2$, homolytic fission of one Xe-F bond is predicted to dominate the gas-phase dynamics.[6] Facile migration of photolytically released F atoms occurs in rare-gas matrices,[13] but reaction with the solvent may limit the F-atom mobility in organic solvents.

Application of XeF in excimer lasers provided some original impetus for studying the ground and electronically excited XeF states.[10,14–17] Figure 1 shows the electronic states of XeF that are important in 266-nm photolysis of $XeF_2$. One-photon absorption by $XeF_2$ leads to ground-state XeF through Xe-F bond cleavage, and its strong absorption to the *B* state near 345 nm provides a probe of the XeF photoproduct.[2] The ground state is bound by about 1200 $cm^{-1}$ in the gas phase,[10] and a large fraction of the XeF products remain bound well beyond the timescale of our measurement.[2] The electronically excited states of XeF are ionic in character, and an F atom in the vicinity of XeF perturbs the optically bright *B* state.[18] We use this known shift of the XeF spectrum as a marker for incomplete separation of the condensed-phase products, allowing us to follow with detail the condensed-phase dynamics that occur within the first few ps after photolysis of $XeF_2$.

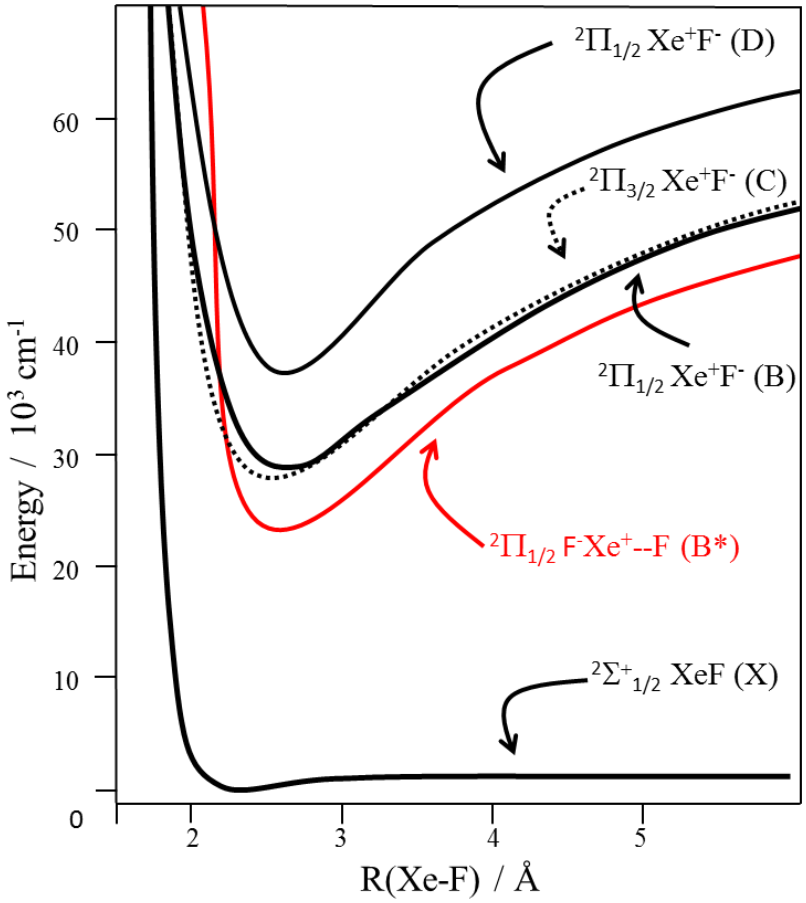


*FIGURE 1. Schematic diagram of the bound, gas phase, electronic states of XeF relevant in this work, adapted from Zerza et al.*[18] *The ion-pair character of the B state makes it susceptible to electronic perturbations. The red curve shows the shift of the B state caused by a neighbouring F atom, first identified by Apkarian and co-workers.*[18]

## II. EXPERIMENTAL APPROACH

### A. *Transient Absorption Spectroscopy*

The ULTRA Facility at the Central Laser Facility of the Rutherford Appleton Laboratory houses the apparatus we used to photolyse $XeF_2$ and to measure electronic-absorption spectra with 1-ps time resolution. The instrumentation used is unchanged from our recent study of chlorine-atom reactions[19] and is described in detail elsewhere.[20] A Ti:sapphire laser operating

at 10 kHz generates both a 266-nm photolysis pulse and a white light continuum (WLC) probe pulse covering 320-700 nm, and an optical delay stage controls the relative timing, $\Delta t$, of their interaction with the liquid sample. A 512-element Si photodiode array measures the intensity of the spectrally dispersed broadband probe pulses. An optical chopper wheel modulates the photolysis pulse at 5 kHz for realtime background subtraction and normalisation.

Imperfect alignment of the beam along the optical delay line that controls the relative timing of photolysis and probe pulses can affect signal intensities at $\Delta t \geq 100$ ps. To compensate for this we use the known excited-state lifetime of phenol in cyclohexane[21] to apply a linear correction factor to the transient $XeF_2$ photolysis data we present. This correction yields long-time kinetics in the $XeF_2$ systems that are consistent with previous measurements.[2] The spectra are not corrected for the temporal chirp in the WLC: instead, data for time delays <1 ps are excluded from analysis.

The solute $XeF_2$ is fragile, and keeping samples colder than 290 K before and during measurements helps ensure its stability. Dried glassware, solvents, and sample holders prevent unwanted side reactions between $XeF_2$ and water. Rapid thermal reaction of the possible contaminant $XeF_4$ with solvent[5] ameliorates its effect on our measurements. Acquiring a pre-determined set of time delays between photolysis and probe pulses in random order further reduces the effects of longer timescale changes in the sample on our measurement. Dilute solutions of 0.25 M $XeF_2$ (>99.9 % trace metal basis, Sigma Aldrich) in dried $CH_3CN$, $CCl_4$, $CDCl_3$, or $CD_2Cl_2$ pass through a sealed flow system. A rastering sample cell, consisting of $CaF_2$ windows separated by a 0.2 mm PTFE spacer, ensures that each laser pulse interrogates a fresh sample volume.

B. *Computational Methods*

Calculations of both the $XeF_2$ and XeF systems enhance our understanding of the $XeF_2$ photophysics. Excited-state CASMPT calculations followed by CASPT2 correction, of the $XeF_2$ potential energy surface use the aug-cc-pVDZ[22] basis set for F atoms and the ECP46MWB effective core potential for Xe. Calculations were implemented with use of the MOLPRO program.[23] This treatment is an effective quasi relativistic model for the large Xe core and has proven successful in modelling the stability of $Au^+$-Xe complexes.[24] We also replicate the XeF *X* and *B* states using known constants[10] to calculate the vibrational wavefunctions through an RKR analysis.[25] The electronic absorption spectrum of vibrationally excited XeF is then simulated through a Frank-Condon analysis with use of the Level programme.[26]

## III. RESULTS AND DISCUSSION

### A. *XeF from $XeF_2$*

The steady state absorption spectrum of gas phase $XeF_2$, is shown in Figure 2, and is fraught with multiple features and possible dissociation products.[27] The lowest energy electronic absorption, which has a maximum near 240 nm, populates the $\Sigma_u$ state and promptly produces XeF(*X*) + F.[2,6] Photolysis at 266 nm, about 4.6 eV of excitation, also makes Xe + $F_2$ and Xe + 2F energetically available, but previous studies have not directly observed these more complicated dissociation pathways.[27] Absorbing two photons, which we show below to be unlikely in our experiment, could produce XeF in electronically excited states.

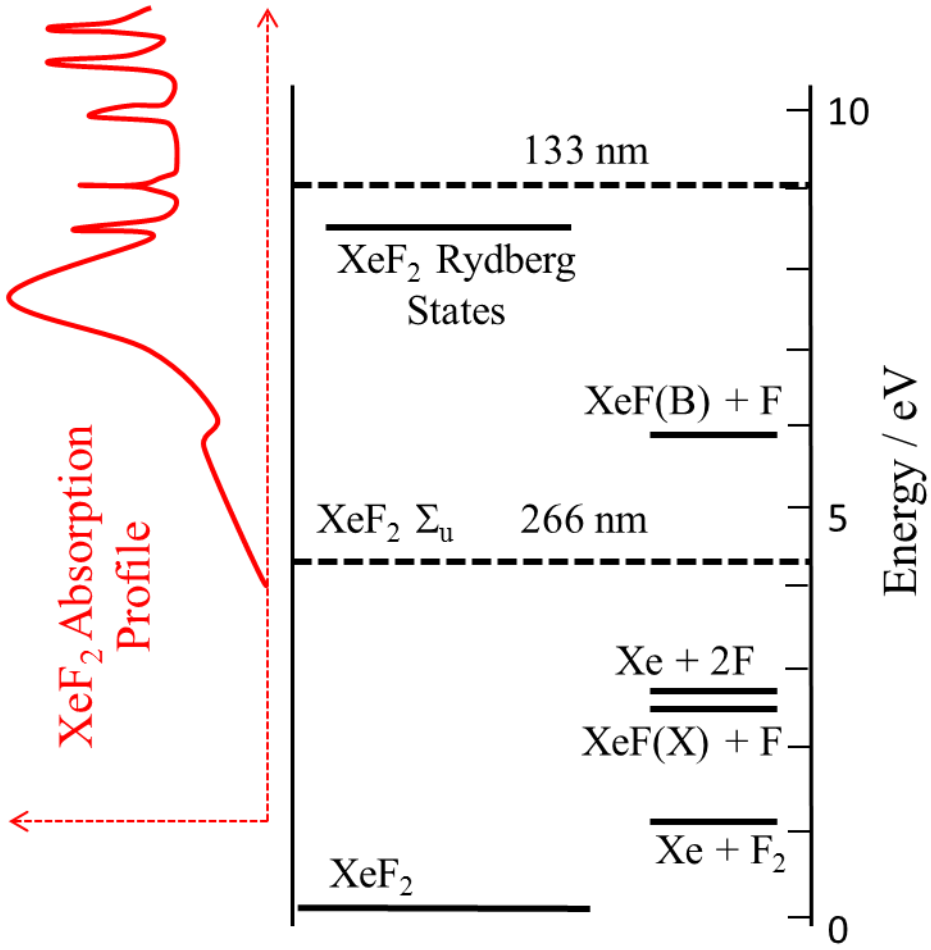

*FIGURE 2. Sketch of the $XeF_2$ absorption spectrum, electronic states, and energy of photoproducts, adapted from Kono et al.*[27] *One- and two-photon absorption (indicated by the horizontal dashed lines) by $XeF_2$ give many energetically accessible photoproducts, but a linear power dependence of the XeF(B─X) feature has confirmed that only one photon processes occur within our experimental setup*

Previous work has identified the condensed-phase XeF absorption spectrum in both steady-state cryogenic matrices[16,28] and in liquid samples of photolysed $XeF_2$.[2] We use these prior assignments to guide the interpretation of our measurements, which are the first to follow this process on the ps to ns timescale. Ground-state XeF isolated in cryogenic rare gas matrices shows a broad absorption feature near 320 nm. This feature is the $B \leftarrow X$ transition, which lies approximately 4000 $cm^{-1}$ lower in energy than in the gas phase.[16,28] Photolysis of $XeF_2$ at 266 nm in $CD_3CN$ produces XeF with a sharp feature near 345 nm.[2] XeF has a 25 μs lifetime in acetonitrile, and our transient absorption spectrum at $\Delta t$ = 500 ps matches the previously measured spectrum at $\Delta t$ = 100 ns.[2] Because the spectrum is largely unchanged between our longest time delay and ns to μs intervals, we take our long-time spectrum to represent the equilibrated XeF photoproduct.

It is necessary to verify that one-photon absorption dominates our condensed-phase study. Photolysis with ns laser pulses at 266 nm and intensities greater than $9\times10^{12}$ $W/cm^2$ saturates the transition to the $\Sigma_u$ state and ensuing absorption of a second photon produces electronically excited XeF(*B*) and an F atom.[29] Our photolysis intensity of about $1\times10^{12}$ $W/cm^2$ is ten times smaller than the onset of two-photon absorption.[29] The integrated area of the transient absorption feature at $\Delta t$ = 500 ps, which measures XeF from photolysis of $XeF_2$, as a function of photolysis pulse energy,[2] produces a linear dependence within the range

$0.25 – 2.5 \times 10^{12}$ W/cm$^2$, spanning more than an order of magnitude of attenuation *below* the onset of two-photon absorption.[29] We therefore conclude that transient signals measured and shown here result from one-photon absorption leading to the XeF(*X*) + F photodissociation pathway.

Decomposition to Xe+$F_2$ is a lower energy channel than XeF + F production and so might compete following UV excitation of $XeF_2$. We discount contributions to the transient spectra from this pathway because $F_2$ absorbs only weakly in the observable, 320-700 nm region[30] and the strong Xe--$F_2$ $\rightarrow$ $Xe^+$--$F_2^-$ charge transfer band lies to much shorter wavelength. In liquid xenon, for example, the band is observed below 185 nm.[31,32]

*B. Electronic States of XeF and FXe-F*

The XeF *B*–*X* absorption was also observed in $CD_2Cl_2$, $CDCl_3$ and $CCl_4$ solvents and the maximum of each spectrum shifts monotonically with the dielectric constant of the solvent, $\varepsilon_r$. The polar solvents preferentially solvate the ion-pair *B* state of XeF relative to its *X* state,[18] decreasing the energy of the transition. Apkarian and co-workers[18] showed that the Onsager reaction-field description of the stabilization of a point dipole in a dielectric cavity[33,34] captures the essence of the energy shift of the *B* state.[18] In this model, the change in energy of the solvated *B* state relative to the gas phase, $\Delta E$, is

$$\Delta E = -\frac{1}{4\pi\varepsilon_0 a^3}\frac{2(\varepsilon_r-1)}{2\varepsilon_r+1}\mu^2, \qquad (1)$$

with the dipole moment of the *B* state, $\mu$, and radius, $\alpha$, of the host cavity in the solvent as the only molecular parameters. The XeF(*B*–*X*) absorption spectra from the current work fit the general trend of Equation 1, as shown in Figure 3, providing a two-fold lesson that we carry forward to our interpretation of the transient electronic absorption spectra in the next section.

First, because Equation 1 only applies to the *B* state of XeF yet gives reasonable agreement with observed trends, electrostatic effects perturb the ion-pair *B* state more than the covalent ground state. Second, we can use the time evolution of the XeF absorption spectrum as a reporter of the dynamic local electrical environment[18] as the system evolves from $XeF_2$ to photolysis products.

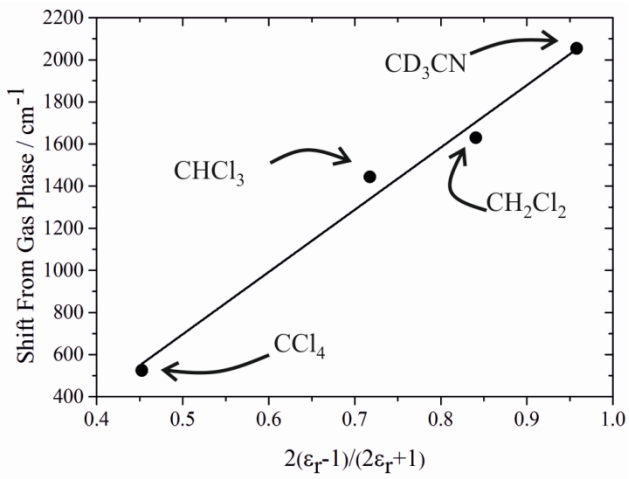


*FIGURE 3. Stabilisation energy of the XeF B state as a function of the solvent dielectric constant, $\varepsilon_r$. The filled circles are the energy difference from the gas phase as determined by the maximum of the XeF(B─X) absorption at $\Delta t$=500 ps. The solid line shows that the model of Equation1 reproduces the trend in the data.*

One factor perturbing the XeF spectrum is the electronegative F-atom photoproduct of $XeF_2$. Because some photolysis events lead to incomplete separation of the XeF and F fragments, we observe the spectral signatures of the metastable FXe-F complex. This complex is stable in rare-gas matrices at 20 K and indeed influences the *B* state.[18] Apkarian and co-workers first described how the F atom decreases the energy gap between the XeF(*X*) and XeF(*B*) states and labelled this altered state XeF(*B**),[18] shown by the red line in Figure 1.

Figure 4 shows the results of our calculations of the isolated FXe-F complex, as detailed in the Experimental Approach, and they provide an extension of the original description of the electronic states in the FXe-F complex.[18] We label the states of the complex as they correlate

to the *X*, *A*, and *B* states of XeF at large FXe-F separation. The figure displays the results of calculations with linear $F_A$-Xe-$F_B$ geometries and a fixed $F_A$-Xe bond length at its calculated minimum of 2.3 Å, which is in agreement with previous work.[14,15] These calculations show no barrier to association back to bound $XeF_2$, but the FXe-F complex is known to be stable in Ar and Ne matrices.[18] Stabilisation of the *B*-state by approach of an F atom collinear to the diatomic axis, and a reduction in the gap between the *B* and *X* states are consistent with the red shifted *B**-*X* absorption band

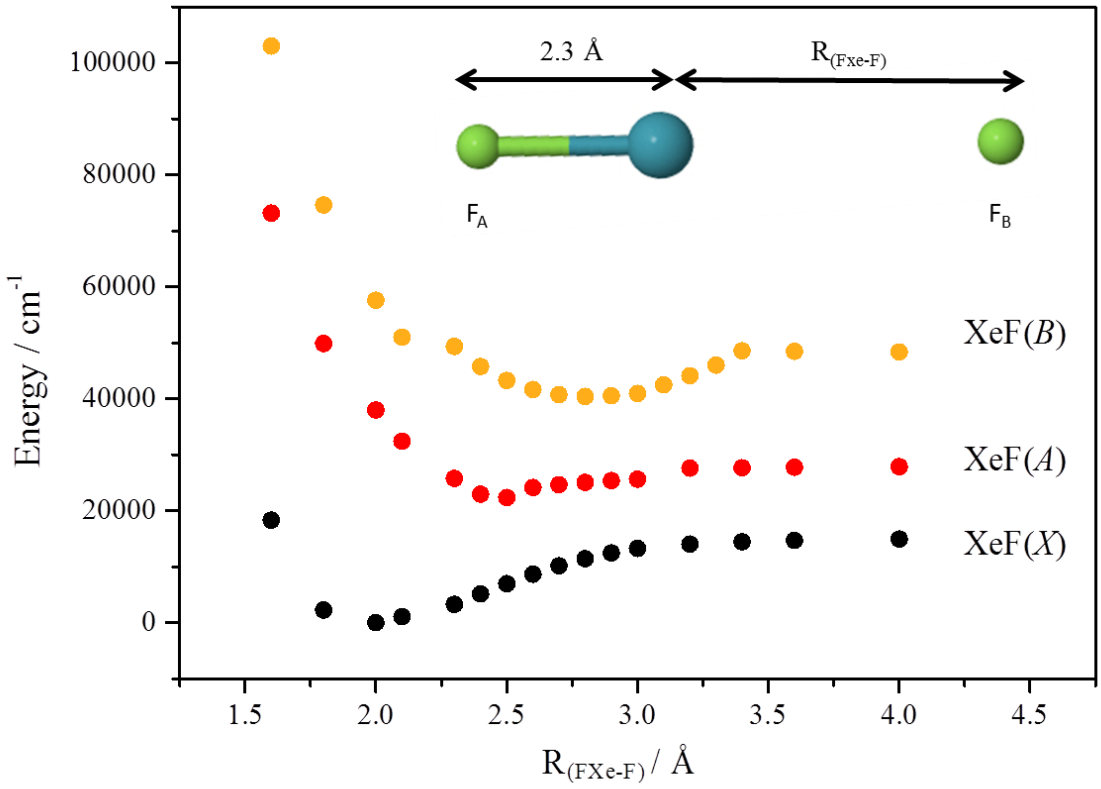


*FIGURE 4. Calculated electronic states of the FXe-F complex in linear F-Xe-F geometries. The labels for the states of the complex match the states of isolated XeF to which they correlate. The B state in the complex is the same as the XeF(B*) of Zerza et al.*[18] *Association to bound $XeF_2$ is barrierless at this level of theory. Bent F-Xe-F configurations lead to repulsive states.*

Avoided crossings with repulsive states derived from the XeF(*X*) and XeF(*A*) potentials are observed in the *A* and *B* states of the complex. Calculations with an FXe-F bond angle of 90° produce purely repulsive potentials over all states. These repulsive states show that the complex has a preferred linear geometry and that the stabilization is likely to occur through the overlap of the XeF $^2\Sigma^+$ state with the F $p_z$ orbital.

*C. Photolysis of $XeF_2$ in Acetonitrile*

We have established that condensed-phase photolysis of $XeF_2$ leads to FXe-F bond cleavage, and Figure 5 shows the resultant time-resolved transient electronic absorption spectra in deuterated acetonitrile. Promptly after photolysis, a broad feature that extends from the lowest wavelength that we probe to about 450 nm dominates the spectrum. During the subsequent 25 ps, this prompt feature shifts to lower wavelength and decays as a second, sharp feature appears near 345 nm, showing signatures of a isosbestic point. The second feature persists from about 50 to 2500 ps in our measurement, and we have demonstrated above that it belongs to the previously assigned *B*–*X* transition of XeF.[2]

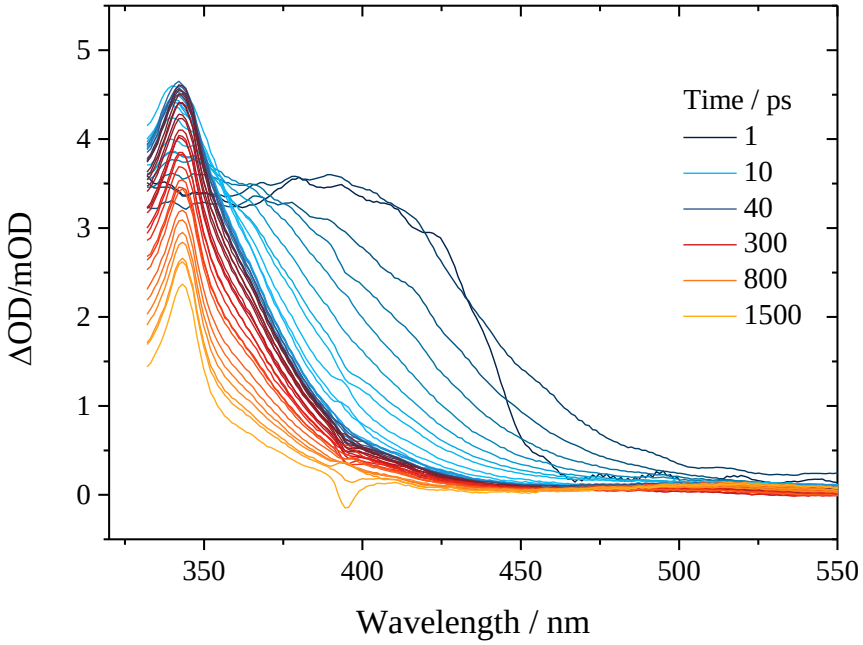

*FIGURE 5. Time-resolved transient absorption spectrum following 266 nm photolysis of $XeF_2$ in acetonitrile. The sharp feature near 345 nm results from B–X absorption by XeF. The released F atom perturbs the B state of XeF, causing the prompt, broad feature which is observed at time delays less than 10 ps. The dip seen at ~390-400 nm is caused by scattered second-order diffraction of the photolysis light into the spectrometer.*

The spectrum of the feature at 425 nm and its evolution into the 345-nm XeF band are consistent with prompt formation and decay of the FXe-F complex, but not with alternative assignments such as to Xe-$F_2$ for reasons outlined earlier. We make further arguments for the assignment here and comment on its implications in condensed-phase reactions below. The 5500 $cm^{-1}$ shift to lower energy of XeF(*B**–*X*) relative to the XeF(*B*–*X*) transition is larger than the 2740 $cm^{-1}$ shift reported for FXe-F in Ne and 4245 $cm^{-1}$ in Ar.[18] The difference between these two matrices indicates that the more polarisable medium of Ar more effectively stabilises the *B** state, lowering the energy of the transition. It is therefore reasonable to propose that the greater polarisability of acetonitrile, decreases the XeF(*B**–*X*) energy gap further.

The shape of the prompt feature, which extends from the visible to the ultraviolet, is consistent with electronic states of FXe-F shown in Figure 4. At an FXe-F distance of about 2.9 Å, the calculated *B**-*X* energy gap goes through a minimum that corresponds to a 361-nm long-wavelength absorption cutoff. Longer and shorter distances have larger energy gaps, which could account for the broad extension of the feature to shorter wavelength. The Franck-Condon-active mode of the absorption is likely to be stretching between the $F_AXe$ pair, which is orthogonal to the plotted coordinate. Thus, the intensity of the transition could remain relatively constant over all Xe-$F_B$ distances, reflected by the flat-topped prompt absorption. The overestimate of the energy gap, however, is attributed to the gas-phase nature of the calculation. Exploring the effects of other FXe-F degrees of freedom or the solvent is

beyond the scope of the current work, but we expect the general trends presented in these isolated molecule calculations to apply to the current condensed phase study.

Absorption to the *A* state of XeF may be discounted as a source of the longer wavelength absorption, because it has a gas-phase band origin near 1400 nm.[16] Other candidates for the prompt absorption that we rule out include vibrationally excited XeF, charge-transfer transitions between XeF or F and the solvent or between Xe atoms and $F_2$ (see earlier), and excited-state absorptions of XeF or $XeF_2$. A spectral simulation of the XeF *X* and *B* states using previously derived spectroscopic constants[10,18] shows that populating up to the highest bound vibrational level of XeF shifts the gas phase spectrum by only 14 nm, which is incongruous with our observation. Both XeF-to-$CD_3CN$ and F-to-$CD_3CN$ charge-transfer transitions have calculated high intensity transitions outside our probe range as discussed in the electronic supplementary information (ESI).

The *B* state of XeF has a 14 ns gas phase lifetime,[35] raising the possibility of an excited state absorption. As Figure 2 describes, the absorption of 1 photon at 266 nm does not allow for population of an electronically excited state of XeF, which discounts the absorption out of this excited state. Equally excited state absorptions of $XeF_2$ may be removed as a possible source of the long wavelength absorption, as no energetically accessible bound states of $XeF_2$ are known to exist.[27]

Global fitting of the transient absorption spectra in Figure 5 through deconvolution of the prompt XeF(*B**─*X*) and long-lived XeF(*B*─*X*) spectral signatures provides ready analysis of the kinetics of the system. At all times after photolysis *t*, we fit the spectrum, $S(\lambda,t)$ to a sum of two spectral features,

$$S(\lambda, t) = A(t)P(\lambda) + [B(t)\,\mathrm{erf}(\lambda) + S_0(t)]. \qquad (2)$$

Because the spectrum at $\Delta t \geq 500$ ps results from only XeF($B$─$X$) absorption, and our spectral simulation described in the ESI indicates that the XeF($B$─$X$) spectrum changes inappreciably with excess internal energy, we treat the long-time spectrum as the basis for fitting the time-invariant XeF($B$─$X$) spectrum, $P(\lambda)$. The function $P$ is a Voigt profile fit to the average 1000 ps $\leq \Delta t \leq$ 1500 ps spectra. We use an error function to model the evolution of the prompt spectrum not to describe a particular model, but because it requires few floating parameters and captures the general appearance of this feature that extends beyond our probe range. The amplitude of the long-time absorption, $A(t)$, directly reports on the free XeF population, and an integral of the error function with combined offset and amplitude scaling factor $B$(t) provides an estimate of the FXe-F complex population.

The deconvolved time evolution of the XeF and FXe-F features, shown in Figure 6 as $A(t)$ in black and $\int_{330}^{600} [B(t)\,\mathrm{erf}(\lambda) + S_0(t)]\; d\lambda$ in red, faithfully represents the kinetics of the raw spectra of Figure 5. The rapid rise of the XeF($B^*$─$X$) feature shows that the FXe-F complex forms within our time resolution, which is about 1 ps. It is also possible for the liberated F atom to escape the vicinity of the XeF co-fragment directly, similar to the facile migration reported for F atoms in rare gas matrices.[13] The kinetic scheme used to model the data is described below, with fits to the model shown as solid lines in Figure 6.

$$XeF_2 \xrightarrow{k_1} \text{FXe-F Complex}$$

$$XeF_2 \xrightarrow{k_2} XeF(X) + F$$

$$\text{XeF-F Complex} \xrightarrow{k_3} XeF(X) + F \text{ (or DF from reaction with solvent)}$$

The kinetic model described allows for initial photodissociation of $XeF_2$ to produce either the FXe-F complex (with rate coefficient $k_1$) or XeF($X$) and an escaped F atom ($k_2$). The complex

can subsequently dissociate to form XeF(*X*)+F or react with the solvent ($k_3$), and we observe both a rise in XeF(*B*─*X*) absorption and build-up of DF (the latter by transient IR absorption spectroscopy[36]). The model is fitted to the time-dependent relative yields of XeF(*X*) and FXe-F by numerical integration.

The above scheme neglects some plausible competing loss processes for the FXe-F complex. For example, work in Ar and Ne liquids observed $XeF_2$ growth from FXe-F decay, although this pathway was cut off upon matrix isolation. This recombination of the FXe-F complex is not included explicitly in our analysis because we have no spectral signature for $XeF_2$ recovery. Similarly, our experiments are insensitive to reactive decomposition of FXe-F to Xe + $F_2$ because the charge-transfer band is outside our spectral window, while the near-UV band of $F_2$ is weak and we see no evidence for build-up of this stable molecule in our spectra. However, we recognise that these unobserved pathways could contribute to the magnitude of $k_3$ as additional loss pathways for FXe-F. Fits of the experimental absorption band intensities to the kinetic model produce the rate coefficients reported in Table 1.

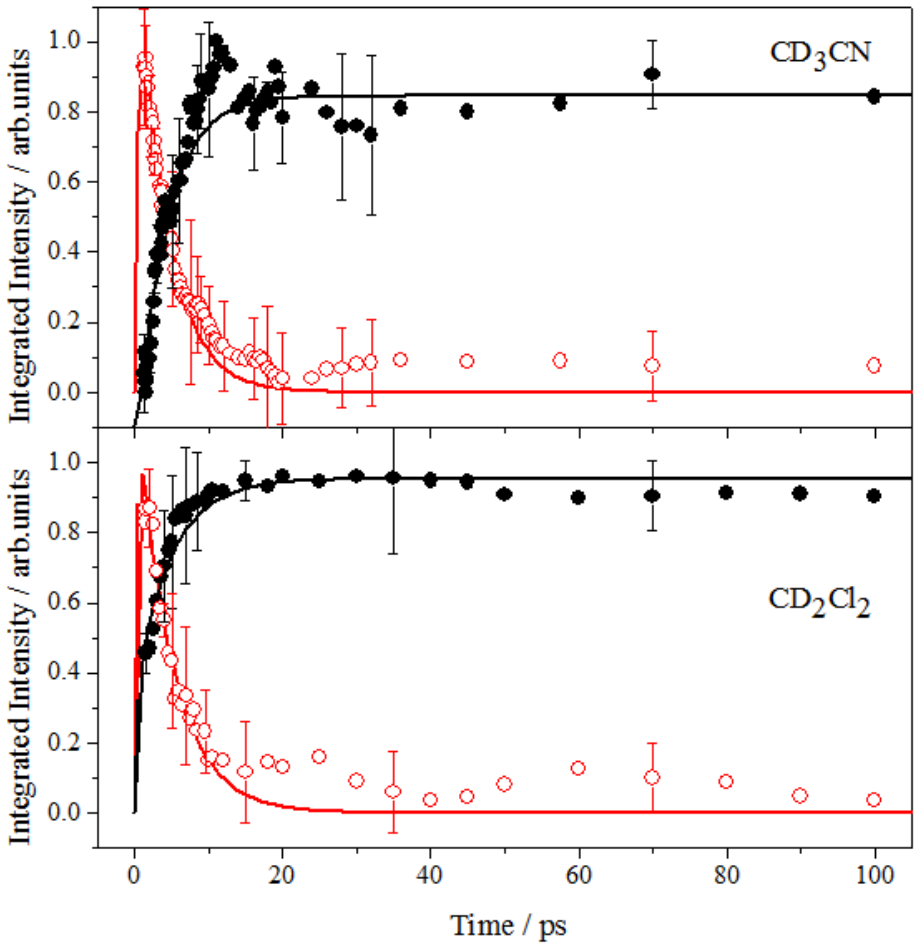


*FIGURE 6. Time-evolution of FXe-F complex (red) and XeF (black) formed from the photolysis of $XeF_2$ at 266 nm in $CD_3CN$ and $CD_2Cl_2$ solvents. Intensities are extracted by a global fit to Equation 2 and subsequently normalised. Solid lines represent the fit to the kinetic model described within the text. The complex rises promptly after photolysis of $XeF_2$ and decays during the first 5 ps. Bare XeF grows with a similar time constant.*

TABLE 1. Rate coefficients extracted from a numerically integrated fit to the kinetic scheme described within the text. Uncertainties quoted are 2 SD.

| **Solvent** | **$k_1$ / $ps^{-1}$** | **$k_2$ / $ps^{-1}$** | **$k_3$ / $ps^{-1}$** |
|---|---|---|---|
| **$CD_3CN$** | 4.2 ± 0.3 | 0 | 0.25 ± 0.01 |
| **$CD_2Cl_2$** | 0.73 ± 0.66 | 0.63 ± 0.33 | 0.22 ± 0.04 |

*Dynamics of Photoproducts*

The rate coefficients in Table 1 are consistent with the dissociation of $XeF_2$ yielding XeF and F, either as a complex or as separated fragments, in less than 1 ps. It is difficult to make an assessment of branching among the prompt photoproduct pathways because the breadth of the prompt feature obscures the region where XeF absorbs most strongly. Furthermore, we do not probe the full FXe-F spectrum, and so we detect only a portion of these products. The decay of this feature may not occur uniformly over all wavelengths, and relative oscillator strengths are not known. The values of $k_1$ and $k_2$ are not well determined because of the 1-ps experimental time resolution. For $CD_3CN$ solutions, the low XeF band intensity in the first few ps after photolysis, creating a negligible rate coefficient for direct production of separated XeF and F, may result from two different factors.

First, if very few F atoms escape the solvent cage ballistically, and nearly all remain trapped within the cage, most of the prompt photoproduct will appear as the FXe-F complex. Small atoms and fragments such as H and CN are known to find their way directly through the solvent cage, [7] [37,38] and F atoms show high mobility in inert matrices,[13] so we expect some

fraction of direct F-atom separation. However, different solvents have a significant influence upon the quantum yield of in-cage recombination. Highly polar solvents such as $H_2O$ show large in-cage recombination quantum yields of ~70 % for ICN photolysis, in comparison to ~30 % in the less polar $CHCl_3$.[39] It is thus reasonable to expect a large proportion of the XeF and F fragments to become trapped within the $CD_3CN$ solvent cage immediately after dissociation.

Second, the impulse of photolysis may impart so much rotational and vibrational energy in the XeF fragment that broadening to the XeF(*B*─*X*) absorption, estimated to be as large as 40 nm FWHM, may occur (ESI). We are unable to separate any such broadened XeF signal from the FXe-F complex feature and therefore cannot make a direct assessment of the importance of this process.

Loss of FXe-F complexes may follow a few competing pathways, of which one is geminate recombination to $XeF_2$. In the previous work that identified the FXe-F complex,[18] the rigid Ar or Ne matrix at 20 K prevented relaxation to linear $XeF_2$, suggesting a small barrier to recombination. Our time-resolved measurements detect FXe-F that is prevented from reforming $XeF_2$, but cannot discriminate between dynamical or energetic causes. However, the commensurate decay of the FXe-F band and growth of the XeF feature, and the near-isosbestic point evident in Figure 5 hint that a significant proportion of the FXe-F survives recombination and instead decays by other routes.

The delayed cage escape and reactive pathways would be expected to have individual rates that depend upon the complex stability and any barrier to reaction. Time-resolved infra-red absorption spectra, reported elsewhere,[36] show build-up of DF product on a timescale that is consistent with the decay of the FXe-F band and rise of the XeF(*X*) band intensities. We conclude that the reaction of the F atom with the solvent is a substantial loss pathway for the

complex, and the rate coefficient $k_3$ represents the sum of this reactive loss, the dissociation of the complex and its recombination to $XeF_2$.

*E. Photolysis of $XeF_2$ in Chlorinated Solvents*

The transient absorption spectra in Figure 7 result from $XeF_2$ photolysis in $CD_2Cl_2$, $CDCl_3$, and $CCl_4$ solvents. Photolysis of these chlorinated solvents at 266 nm also produces transient photoproducts with absorption features in the UV/Vis region.[19,41,42] Subtracting those features from our transient spectra with $XeF_2$, acquired under identical conditions, produces signals resulting only from solute-dependent photo-chemistry.[19,42] In all these chlorinated solvents, it is evident that the majority of the photolysis of $XeF_2$ occurs in less than a picosecond.

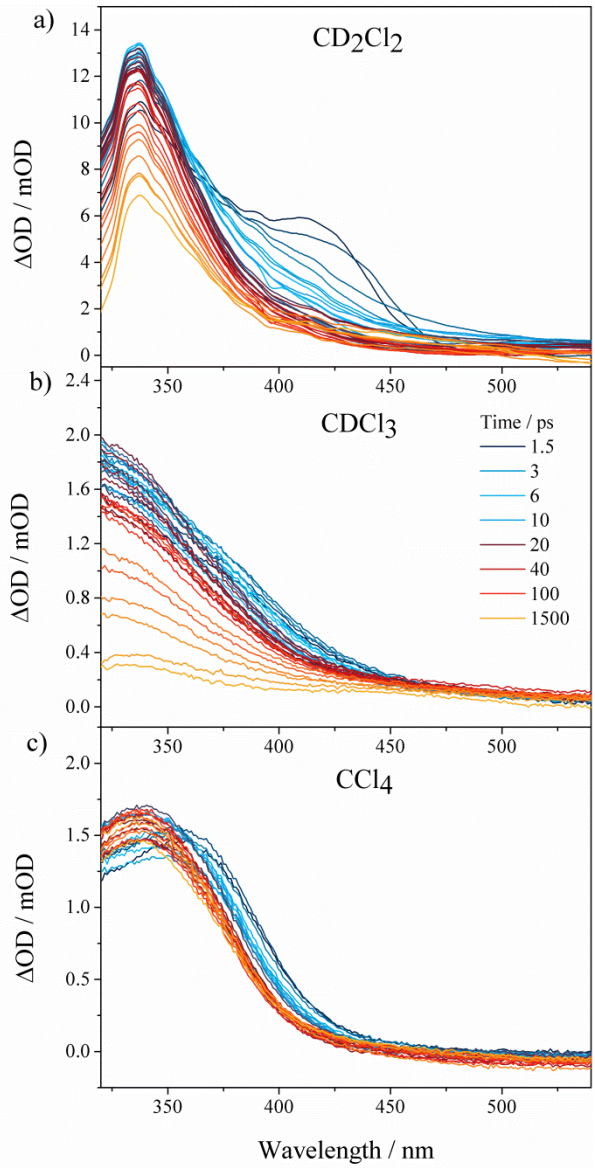


*FIGURE 7. Time resolved transient absorption spectra following 266 nm photolysis of $XeF_2$ in a) $CD_2Cl_2$, b) $CDCl_3$ and c) $CCl_4$. The late time spectra correspond to XeF(X) absorption. The prompt broad feature in the $CD_2Cl_2$ data is attributed to the FXe-F complex. Absorptions caused by the 266 nm photolysis of these chlorinated solvents have been removed.*

We fit the transient spectra in $CD_2Cl_2$, but not the other two solvents, to Equation 2 because there is definite separation between the two transient features. The integrated intensities are then simultaneously fitted to the kinetic model described above, as shown in Figure 6**.** Unlike in acetonitrile, the XeF(*X*) feature near 350 nm appears promptly after photolysis in these

solvents and the FXe-F complex is not as evident in $CDCl_3$ or $CCl_4$. Less clearcut signatures of the complex in these two solvents may be explained by shifts in the FXe-F band to shorter wavelength, a decrease in the branching ratio of complex formation, or an increase in the rate of the loss of the complex.

The rate coefficients extracted from the fit of the integrated band intensities following photolysis of $XeF_2$ in $CD_2Cl_2$ are displayed in Table 1. The direct production of XeF(*X*) shows a significant rate coefficient of $0.63 \pm 0.33$ $ps^{-1}$, while the complex decay shows a time constant similar to that for $XeF_2$ photolysis in acetonitrile. The near identical timescales for complex loss suggest that the stability of the complex to decay (whether by reaction or other pathways discussed earlier) is unchanged upon changing solvent. Reaction with the $CD_2Cl_2$ is most likely to produce DF because we see no evidence for the $B - X$ absorption band of ClF near 480 nm[43] in the transient spectra. The known selectivity of gas-phase reactions of F atoms with chloroform and dichloromethane supports this deduction.[44]

Any difference in the observed FXe-F complex yields between the chlorinated solvents and acetonitrile may result from two distinct mechanisms:

1) The photolytically produced F atom immediately escapes from the solvent cage. Ballistic escape can be affected by the ability of the solvent to quench the excess energy from the system, the mobility of F atoms in the solvent, and the strength of the solvent cage.

2) The probability of prompt recombination to $XeF_2$ increases within the chlorinated solvents. However, the origins of any barrier to recombination are uncertain, so we draw no conclusion about this trend.

The XeF molecule is observed to have a nanosecond or longer stability in $CD_3CN$ and $CCl_4$ solvents but there is a substantial loss channel in $CDCl_3$ and $CD_2Cl_2$. We suggest that the XeF reacts with the solvent to produce DF, and our transient IR absorption studies support this

interpretation.[36] Time constants for the loss of the XeF molecule are found to be 800 ± 200 ps in $CD_2Cl_2$ and 350 ± 50 ps within $CDCl_3$.

The XeF *B*─*X* absorption in $CCl_4$ solvent is observed to shift to shorter wavelength with a 4.1 ± 0.3 ps time constant, which may be indicative of vibrational cooling of the XeF. The XeF(*X*) ground state potential supports ~8 vibrational levels. However, in $CD_3CN$ and $CD_2Cl_2$ solvents the FXe-F complex feature obscures any spectral signatures of vibrational relaxation dynamics.

## IV. CONCLUSIONS

Photodissociation of $XeF_2$ in organic solvents produces XeF(*X*) and F with a time constant of less than 1 ps. If confined within the same solvent cage, the nearby photolytically produced F atom perturbs the ionic *B* state of the XeF molecule, which allows the formation of these FXe-F complexes to be observed spectroscopically. Such complexes have previously been observed in Ar and Ne matrices.[18] The FXe-F is expected to be only weakly bound, and the decay of its spectral band provides information on the reactive removal of F atoms. The perturbed XeF(*B**─*X*) spectral band of the FXe-F complex appears immediately after photolysis in $CD_3CN$, while significant free XeF(*X*) is observed promptly in $CD_2Cl_2$. The perturbed signal assigned to the FXe-F decays with a time constant of 4.0 ± 0.2 ps in $CD_3CN$ and 4.5 ± 0.8 ps in $CD_2Cl_2$. Much of the decay of the complex is expected to occur through D atom abstraction reactions with the solvent to produce DF. Spectral features of the FXe-F complex are less clear, or absent, for $XeF_2$ photolysis in $CDCl_3$ or $CCl_4$.

The XeF molecule is stable in $CD_3CN$ and $CCl_4$ solvents for nano- to microseconds. Substantial loss channels of XeF in $CDCl_3$ and $CD_2Cl_2$ solvents are suggestive of reaction with the solvent.

## ACKNOWLEDGMENTS

We thank Dr D.P. Tew, University of Bristol for help with CASPT2 calculations. The Bristol group gratefully acknowledges financial support from the EPSRC (Programme Grant EP/G00224X) and the ERC (Advanced Grant 290966 CAPRI). Experimental measurements were conducted at the ULTRA facility which is supported by STFC (Facility Grant ST/501784).

1. I. Benjamin and K. R. Wilson, *J. Chem. Phys.*, 1989, **90**, 4176–4197.

2. G. Bucher and J. C. Scaiano, *J. Am. Chem. Soc.*, 1994, **116**, 10076–10079.

3. J. C. Scaiano, G. Bucher, M. Barra, D. Weldon, and R. Sinta, *J. Photochem. Photobiol.*, 1996, **102**, 7–11.

4. M. Tramšek and B. Žemva, *Acta Chim. Slov.*, 2006, **53**, 105–116.

5. M. A. Tius, *Tetrahedron*, 1995, **51**, 6605–6634.

6. H. Kunkely and A. Vogler, *Inorganica Chim. Acta*, 2004, **357**, 2407–2409.

7. T. A. A. Oliver, Y. Zhang, M. N. R. Ashfold, and S. E. Bradforth, *Faraday Discuss.*, 2011, **150**, 439–458.

8. S. J. Harris, D. Murdock, Y. Zhang, T. A. A. Oliver, M. P. Grubb, A. J. Orr-Ewing, G. M. Greetham, I. P. Clark, M. Towrie, S. E. Bradforth, and M. N. R. Ashfold, *Phys. Chem. Chem. Phys.*, 2013, **15**, 6567–6582.

9. G. Black, R. L. Sharpless, D. C. Lorents, D. L. Huestis, and R. A. Gutcheck, *J. Chem. Phys.*, 1981, **75**, 4840–4846.

10. P. C. Tellinghuisen, J. Tellinghuisen, J. A. Coxon, J. E. Velazco, and D. W. Setser, *J. Chem. Phys.*, 1978, **68**, 5187–5198.

11. W. Dukat, J. H. Holloway, E. G. Hope, P. J. Townson, and R. L. Powell, *J. Fluor. Chem.*, 1992, **62**, 293–296.

12. A. J. Orr-Ewing, *J. Chem. Phys.*, 2014, **140**, 090901–12.

13. V. A. Apkarian and N. Schwentner, *Chem. Rev.*, 1999, **99**, 1481–1514.

14. P. C. Tellinghuisen and J. Tellinghuisen, *J. Phys. Chem. A*, 2002, **106**, 8317–8322.

15. T. H. Dunning and P. J. Hay, *J. Chem. Phys.*, 1978, **69**, 134–149.

16. B. S. Ault and L. Andrews, *J. Chem. Phys.*, 1976, **64**, 3075–3076.

17. M. Krauss and B. Liu, *Chem. Phys. Lett.*, 1976, **44**, 257–260.

18. G. Zerza, G. Sliwinski, N. Schwentner, G. J. Hoffman, D. G. Imre, and V. A. Apkarian, *J. Chem. Phys.*, 1993, **99**, 8414–8423.

19. F. Abou-Chahine, T. J. Preston, G. T. Dunning, A. J. Orr-Ewing, G. M. Greetham, I. P. Clark, M. Towrie, and S. A. Reid, *J. Phys. Chem. A*, 2013, **117**, 13388–13398.

20. G. M. Greetham, P. Burgos, Q. Cao, I. P. Clark, P. S. Codd, R. C. Farrow, M. W. George, P. Matousek, A. W. Parker, M. R. Pollard, A. Robinson, Z. Xin, and M. Towrie, *Appl. Spectrosc.*, 2010, **64**, 1311–1319.

21. Y. Zhang, T. A. A. Oliver, M. N. R. Ashfold, and S. E. Bradforth, *Faraday Discuss.*, 2012, **157**, 141–163.

22. T. H. Dunning, *J. Chem. Phys.*, 1989, **90**, 1007–1023.

23. H. J. Werner, P. J. Knowles, G. Knizia, F. R. Manby, M. Schütz, P. Celani, T. Korona, R. Lindh, A. Mitrushenkov, G. Rauhut, K. R. Shamasundar, T. B. Adler, R. D. Amos, A. Bernhardsson, A. Berning, D. L. Cooper, M. J. O. Deegan, A. J. Dobbyn, F. Eckert, E. Goll, C. Hampel, A. Hesselmann, G. Hetzer, T. Hrenar, G. Jansen, C. Köppl, Y. Liu, A. W. Lloyd, R. A. Mata, A. J. May, S. J. McNicholas, W. Meyer, M. E. Mura, A. Nicklass, D. P. O'Neill, P. Palmieri, K. Pflüger, R. Pitzer, M. Reiher, T. Shiozaki, H. Stoll, A. J. Stone, R. Tarroni, T. Thorsteinsson, A. Wolf, and M. Wang, MOLPRO 2010.

24. D. Schroder, H. Schwartz, J. Hrusak, and P. Pyykko, *Inorg. Chem.*, 1998, **37**, 624–632.

25. R. J. Le Roy, RKR1 2.0, 2004.

26. R. J. Le Roy, Level 8.0, 2007.

27. M. Kono and K. Shobatake, *J. Chem. Phys.*, 1995, **102**, 5966–5978.

28. B. S. Ault and L. Andrews, *J. Chem. Phys.*, 1976, **65**, 4192–4201.

29. G. W. Loge and J. R. Wiesenfeld, *J. Chem. Phys.*, 1981, **75**, 2795–2799.

30. H. Keller-Rudek, G. K. Moortgat, R. Sander, and R. Sörensen, The MPI-Mainz UV/VIS Spectral Atlas of Gaseous Molecules of Atmospheric Interest.

31. M. E. Fajardo, V. A. Apkarian, A. Moustakas, H. Krueger, and E. Weitz, 1988, 357–360.

32. H. Kunttu, E. Sekreta, and V. A. Apkarian, *J. Chem. Phys.*, 1991, **94**, 7819.

33. L. Onsager, *J. Am. Chem. Soc.*, 1936, **58**, 1486–1493.

34. N. Henriksen and F. Hansen, *Theories of Molecular Reaction Dynamics*, Oxford Graduate Texts, 2008.

35. J. G. Eden and R. W. Waynant, *Opt. Lett.*, 1978, **2**, 13–5.

36. G. T. Dunning, D. R. Glowacki, S. J. Greaves, T. J. Preston, G. M. Greetham, I. P. Clark, M. Towrie, and A. J. Orr-Ewing, *Publ.*

37. I. Benjamin, *J. Chem. Phys.*, 1995, **103**, 2459–2471.

38. D. Raftery, E. Gooding, A. Romanovsky, and R. M. Hochstrasser, *J. Chem. Phys.*, 1994, **101**, 8572–8579.

39. A. C. Moskun and S. E. Bradforth, *J. Chem. Phys.*, 2003, **119**, 4500–4515.

40. A. C. Crowther, S. L. Carrier, T. J. Preston, and F. F. Crim, *J. Phys. Chem. A*, 2008, **112**, 12081–9.

41. G. Maier, H. P. Reisenauer, J. Hu, L. J. Schaad, and B. A. Hess, *J. Am. Chem. Soc.*, 1990, **112**, 5117–5122.

42. T. J. Preston, M. A. Shaloski, and F. F. Crim, *J. Phys. Chem. A*, 2013, **117**, 2899–907.

43. A. L. Wahrhaftig, *J. Chem. Phys.*, 1942, **10**, 248–248.

44. M. A. Wickramaaratchi, D. W. Setser, H. Hildebrandt, B. Korbitzer, and H. Heydtmann, *Chem. Phys.*, 1985, **94**, 109–129.